A procedure for the design of nozzles used for the production of turbulent liquid jets

T. W. Davies* and M. K. Jackson**

Where turbulent liquid jets are used for cutting and mining purposes the pressure generated by impact must be maximized. Initial jet behaviour has an important influence on subsequent jet impact pressures at medium range. Nozzle wall boundary layer history has a strong influence on the initial jet, and certain boundary layer features can be linked to poor jet performance. The procedure outlined in this paper was developed to eliminate new nozzle designs or changes in operating conditions on the grounds of badly behaved nozzle boundary flow. The design procedure consists of a potential flow analysis and a boundary layer analysis coupled to empirical correlations for boundary layers in accelerated flows. The procedure is exemplified by application to the design of a nozzle to be used for the specific purpose of mining china clay.

Keywords: *nozzle design, jets, accelerating flows*

The motivation to develop the analysis in this paper came from the need to improve the effectiveness of the hydraulic mining of china clay. The clay is mined using jets of water which are projected at the clay-bearing rocks using water cannon devices or monitors. A requirement of the process is that the maximum amount of hydraulic power supplied to the monitors by the pumps be delivered to the working face of the pit via the jet. Nozzle design is one of the factors which determines the efficiency of this process.

A review of the literature[1] on the design of contractions reveals little that is of direct use to the designer of nozzles intended to produce jets of liquid in air. Lohn and Brent[2] surveyed the available analytical tools for nozzle design, and the present work is based upon some of the ideas described in their report. There is a substantial body of empirical knowledge about the features of flow in nozzles and the influence of nozzle flow on the resulting jet. This information is an essential component of the present design procedure, and the interested reader is again referred to Jackson[1] for an exhaustive review. Empirical work used directly in the design method described in this paper includes that of Au[3], which provides a correlation for the entrainment rate of a boundary layer by a converging flow; Schraub and Kline[4], who describe the laminarization of turbulent boundary layers under the influence of an accelerating outer flow; Ramjee and Hussain[5], who describe the phenomenon of turbulence transformation in nozzles; Hoyt and Taylor[6], who describe the effects of transition back to turbulence of a laminarized nozzle boundary layer flow issuing from a nozzle; Murakami and Katayama[7], who describe the effects of nozzle design on discharge coefficients; and Hatton and Osborne[8], who demonstrate the existence of optimum upstream flow conditions for maximum jet throw.

* Department of Chemical Engineering, Exeter University, Exeter EX4 4QF, UK
** Shell International Petroleum Co, The Hague, The Netherlands
Received 23 December 1984 and accepted for publication in final form on 13 May 1985

The approach described here links these empiricisms and will find application in related uses of large water jets and in fire fighting where the throw and coherence of the jet is important. In any particular application certain constraints may limit the freedom of the designer in choosing the ideal geometry for the nozzle and existing inverse solutions to the nozzle flow problem are of no help. (Inverse solutions use the ideal flow equations to define the ideal nozzle shape needed to accomplish a given acceleration, and are often used by wind tunnel designers.) For example, if the object of the hydraulic system as a whole is to transmit power at maximum efficiency (as in Pelton wheel devices), then one can easily demonstrate that the contraction ratio of the nozzle is determined by parameters upstream of the nozzle, such as the friction coefficient in the transmission line between the pump and the nozzle. The problems of fabricating sophisticated nozzle shapes may also exert an important influence on choice of nozzle geometry. Where nozzles are used for drilling boreholes the length (and so the aspect ratio) of the nozzle may be severely limited by the diameter of the borehole.

Under these circumstances, and where the jet has to perform work at a distance, a method of choosing the most appropriate nozzle geometry is desirable. This is because only limited combinations of contraction ratio, aspect ratio, contour shape and surface finish will produce well behaved wall boundary layers for given inlet conditions, and the short range behaviour of liquid jets is a strong function of nozzle boundary layer history.

This paper describes a computational method whereby the flow conditions in a nozzle may be estimated for specified geometry and inlet flow conditions. The method is based on a model of the nozzle flow in which a central axisymmetric accelerating potential flow influences, but is not influenced by an axisymmetric turbulent wall boundary layer flow.

The potential flow field is calculated using a finite difference approximation of the potential flow equation.

The information may be used to eliminate nozzle designs which are unsatisfactory for any of the following reasons.

(1) Flow separation seems likely because of wall pressure overshoot near the nozzle inlet.
(2) Cavitation seems likely because of wall pressure undershoot near the nozzle exit.
(3) The boundary layer seems likely to undergo a marked degree of laminarization before the nozzle exit.

The behaviour of the boundary layer is calculated using the potential flow field as a boundary condition on the equation of motion. The integral form of the boundary layer equation is used together with an empirical expression for the rate of entrainment of the boundary layer fluid by the potential core flow. Simultaneous solution of the boundary layer and entrainment equations is carried out with the boundary layer shape factor as the variable. The distribution of shape factor along the nozzle wall may then be used to study the nature of the boundary layer for any signs of undesirable behaviour. The degree of surface finish required to ensure hydraulically smooth flow may also be predicted.

Inviscid core flow solution

The nozzle flow is idealized by assuming it to be inviscid, incompressible and irrotational. The displacing effect of the boundary layer is neglected. Cylindrical polar coordinates are used to locate the solution nodes of the finite difference scheme. This leads to some additional algebra in setting up the finite difference approximations in the equation of motion since the streamlines, and the nozzle contour, are not coincident with the coordinate system. As usual the approximations for the wall region require special treatment.

The stream equation for the axisymmetric, inviscid, irrotational flow of an incompressible fluid may be obtained as follows:

$$\frac{\partial u}{\partial r}-\frac{\partial v}{\partial x}=0 \quad \text{(irrotationality)} \tag{1}$$

$$\frac{\partial (vr)}{\partial r}+\frac{\partial (ur)}{\partial x}=0 \quad \text{(continuity)} \tag{2}$$

Defining a stream function so that:

$$ru=\frac{\partial \psi}{\partial r} \tag{3}$$

$$rv=-\frac{\partial \psi}{\partial x} \tag{4}$$

and combining Eqs (1) and (2) gives

$$\frac{\partial^2 \psi}{\partial x^2}-\frac{1}{r}\frac{\partial \psi}{\partial r}+\frac{\partial^2 \psi}{\partial r^2}=0 \tag{5}$$

Consider the curvilinear finite-difference grid scheme for internal flow points shown in Fig 1. Employing the normal finite-difference approximations, the derivatives in Eq (5) maybe formulated:

$$\frac{\partial^2 \psi}{\partial r^2}\simeq(\psi_n-2\psi_p+\psi_s)/h^2 \tag{6}$$

$$\frac{\partial \psi}{\partial r}\simeq(\psi_n-\psi_s)/2h \tag{7}$$

$$\frac{\partial^2 \psi}{\partial x^2}\simeq(\psi_e-2\psi_p+\psi_w)/k^2 \tag{8}$$

Substituting Eqs (6), (7) and (8) into (5) and rearranging in terms of ψ_p gives:

$$\psi_p\simeq\frac{\psi_n(1-A)+\psi_s(1+A)+B(\psi_e+\psi_w)}{2(1+B)} \tag{9}$$

Notation

C_c	Coefficient of contraction
C_d	Coefficient of discharge
C_f	Friction factor
d_o	Nozzle diameter
d_{jmin}	Minimum diameter of contracting jet
D	Barrel or pipe diameter
h	Radial grid spacing
H	Shape factor
H'	Mean shape factor
k	Axial grid spacing
K	Number of grid points in r-direction
K_p	Pressure gradient parameter
L_f	Length of nozzle final taper
L_t	Total length of nozzle
$\dot{m}$	Mass flow rate in boundary layer
$\dot{M}$	Mass flow rate per unit nozzle length
N	Number of grid points in x-direction
P	Static pressure
P_o	Nozzle pressure
P_w	Nozzle wall pressure
Q_o	Nozzle volumetric flow rate
r	Radial distance
r_c	Radius defining boundary layer
R	Nozzle wall contour radius
R_o	Nozzle radius
Re_i	Nozzle inlet Reynolds number $=U_iD/v$
Re_θ	Momentum thickness Reynolds number $=U\theta/v$
Re_o	Nozzle exit Reynolds number $=U_od_o/v$
Rp	Relaxation parameter
S	Sublayer thickness
u	Velocity in x-direction
Δu	Difference in velocity between iterations
U	Wall velocity in x-direction
U_i	Nozzle inlet velocity
U_o	Nozzle exit velocity
v	Velocity in r-direction
v^*	Friction velocity
V	Nozzle wall velocity in r-direction
x	Axial distance
y	Distance normal to nozzle wall
δ	Boundary layer thickness
δ^*	Displacement thickness
η	Entrainment parameter
θ	Momentum thickness
μ	Viscosity of water
τ_w	Nozzle wall shear stress
ϕ	Entrainment function
ψ	Stream function

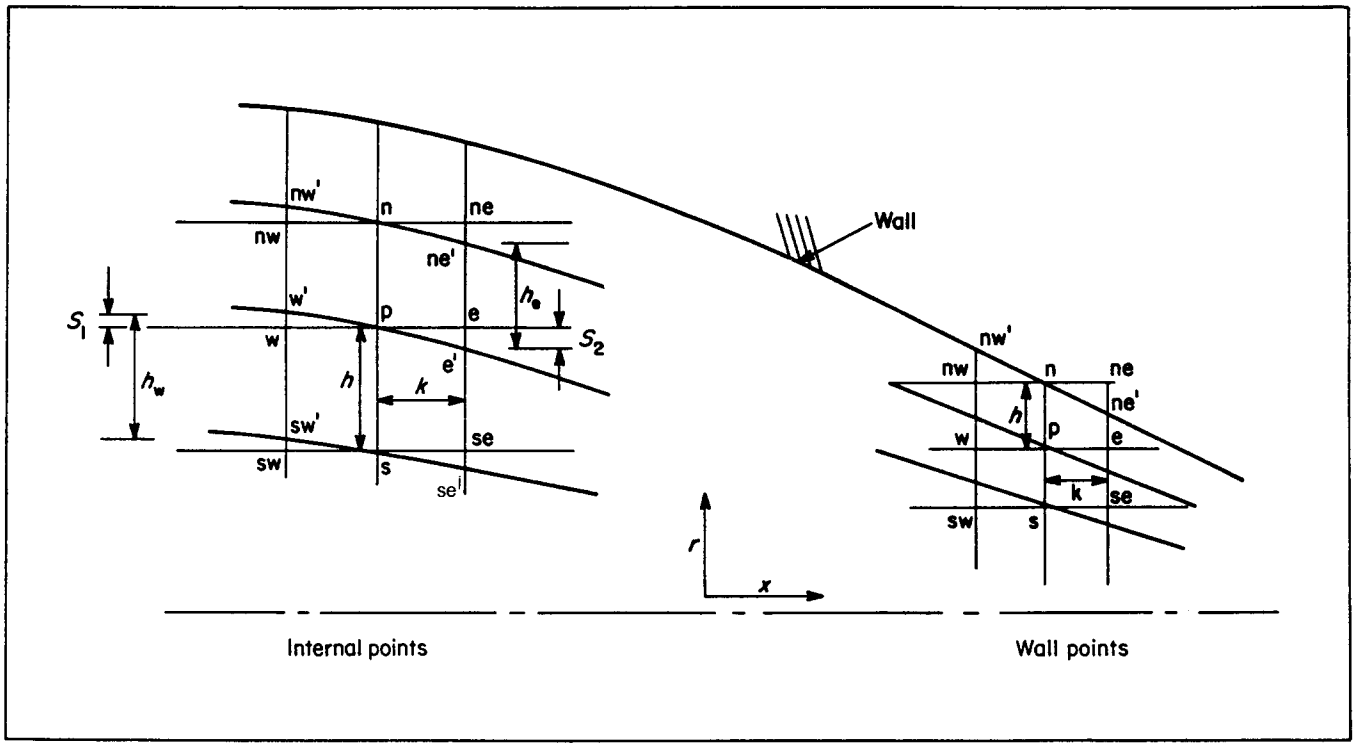

Fig 1 Curvilinear finite difference scheme

where $A=h/(2r)$ and $B=(h/k)^2$. ψ_e and ψ_w are obtained by performing 2nd order Taylor expansions about ψ'_e and ψ'_w respectively (Fig 1).

$$\psi_w \simeq \psi'_w - S_1 \frac{\partial \psi'_w}{\partial r} + \frac{S_1^2}{2} \frac{\partial^2 \psi'_w}{\partial r^2} \tag{10}$$

$$\psi_e \simeq \psi'_e + S_2 \frac{\partial \psi'_e}{\partial r} + \frac{S_2^2}{2} \frac{\partial^2 \psi'_e}{\partial r^2} \tag{11}$$

The derivatives in Eqs (10) and (11) are obtained by consideration of 2nd order Taylor expansions for ψ'_{nw}, ψ'_{sw} and ψ'_{ne}, ψ'_{se} about ψ'_w and ψ'_e, respectively. For example:

$$\psi'_{nw} \simeq \psi'_w + h_w \frac{\partial \psi'_w}{\partial r} + \frac{h_w^2}{2} \frac{\partial^2 \psi'_w}{\partial r^2} \tag{12}$$

$$\psi'_{sw} \simeq \psi'_w - h_w \frac{\partial \psi'_w}{\partial r} + \frac{h_w^2}{2} \frac{\partial^2 \psi'_w}{\partial r^2} \tag{13}$$

Independently eliminating 1st and 2nd order derivatives from Eqs (12) and (13) gives:

$$\frac{\partial \psi'_w}{\partial r} \simeq (\psi'_{nw} - \psi'_{sw})/2h_w \tag{14}$$

$$\frac{\partial^2 \psi'_w}{\partial r^2} \simeq (\psi'_{nw} + \psi'_{sw} - 2\psi'_w)/h_w^2 \tag{15}$$

Similarly:

$$\frac{\partial \psi'_e}{\partial r} \simeq (\psi'_{ne} - \psi'_{se})/2h_e \tag{16}$$

$$\frac{\partial^2 \psi'_e}{\partial r^2} \simeq (\psi'_{ne} + \psi'_{se} - 2\psi'_e)/h_e^2 \tag{17}$$

Substituting Eqs (14) and (15) into (10), and Eqs (16) and (17) into (11), gives:

$$\psi_w \simeq \psi'_w - \frac{S_1(\psi'_{nw} - \psi'_{sw})}{2h_w} + \frac{S_1^2(\psi'_{nw} + \psi'_{sw} - 2\psi'_w)}{2h_w^2} \tag{18}$$

$$\psi_e \simeq \psi'_e + \frac{S_2(\psi'_{ne} - \psi'_{se})}{2h_e} + \frac{S_2^2(\psi'_{ne} + \psi'_{se} - 2\psi'_e)}{2h_e^2} \tag{19}$$

Boundary conditions are set by assuming a uniform velocity profile upstream of the nozzle inlet and downstream of the nozzle exit, and by specifying the wall contour shape. As indicated by Fig 2, the wall shape is parallel upstream from the nozzle inlet and the emerging jet is assumed to contract beyond the nozzle exit with the no-slip condition relaxed. The condition of uniform axial velocity was set to be achieved within a distance of $3k$ from the nozzle exit plane. This computational convenience does not carry any physical significance, and contraction coefficients are not calculable. The procedure produces results for flow within the nozzle which are acceptable for the present purpose. The value of the stream function along the wall streamline is arbitrarily set to unity, and the value of the stream function along the nozzle centre line set to zero. Solution is achieved by a relaxation method, and the new local value of stream function is determined according to:

$$\psi_p = \psi_{p(old)} + Rp(\psi_{p(new)} - \psi_{p(old)}) \tag{20}$$

where $\psi_{p(old)}$ is the value calculated from Eq (20) in the previous iteration, and Rp is the relaxation parameter.

Once the streamline curvature solution has been obtained, the wall velocity distribution may be obtained from:

$$U = \frac{1}{R} \left\{ \frac{d\psi}{dr} \right\}_{wall} \tag{21}$$

$$V = -\frac{1}{R} \left\{ \frac{d\psi}{dx} \right\}_{wall} \tag{22}$$

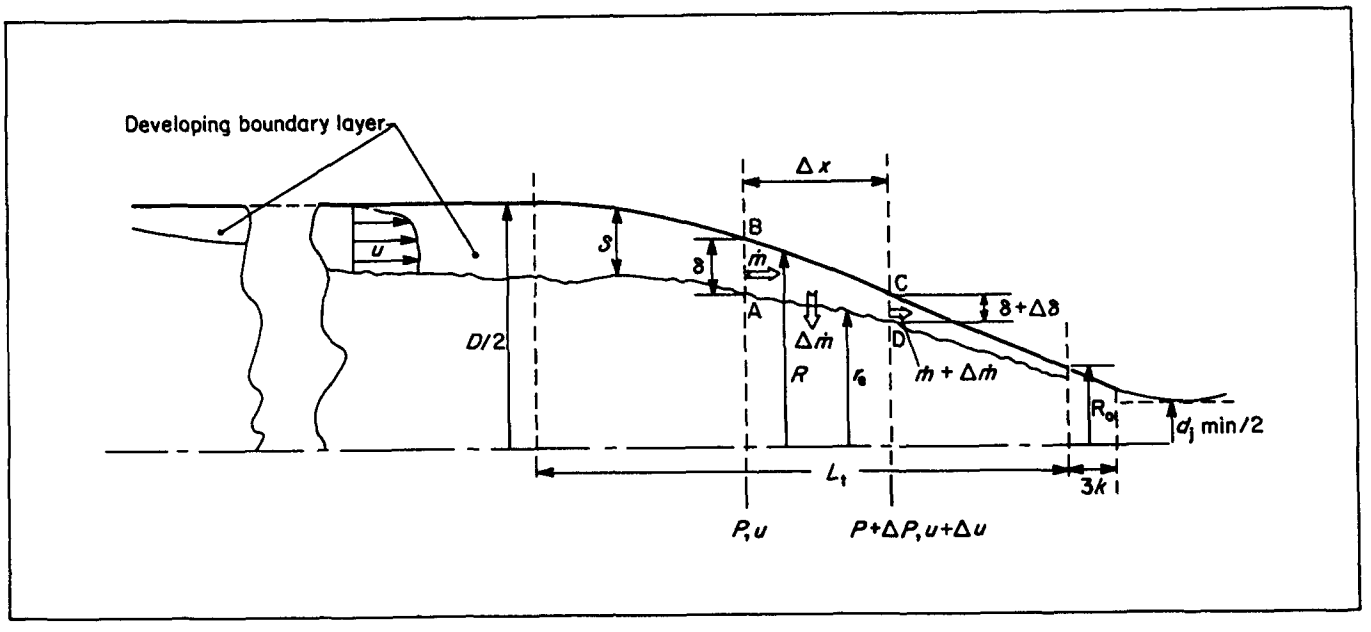

Fig 2 Boundary layer development

Consider the grid scheme for points adjacent to the wall shown in Fig 1. Second order Taylor expansions for ψ_p and ψ_s about ψ_n give:

$$\psi_p \simeq \psi_n + h\frac{\partial\psi_n}{\partial r} + \frac{h^2}{2}\frac{\partial^2\psi_n}{\partial r^2} \tag{23}$$

$$\psi_s \simeq \psi_n - 2h\frac{\partial\psi_n}{\partial r} + 2h^2\frac{\partial^2\psi_n}{\partial r^2} \tag{24}$$

Eliminating $\partial^2\psi_n/\partial r^2$ from Eqs (23) and (24) gives:

$$\frac{\partial\psi_n}{\partial r} \simeq -\frac{4\psi_p + 3\psi_n + \psi_s}{2h} \tag{25}$$

2nd order Taylor expansions for ψ_{nw} and ψ_{ne} about ψ_n give:

$$\psi_{nw} \simeq \psi_n - k\frac{\partial\psi_n}{\partial x} + \frac{k^2}{2}\frac{\partial^2\psi_n}{\partial x^2} \tag{26}$$

$$\psi_{ne} \simeq \psi_n + k\frac{\partial\psi_n}{\partial x} + \frac{k^2}{2}\frac{\partial^2\psi_n}{\partial x^2} \tag{27}$$

Eliminating $\partial^2\psi_n/\partial x^2$ from Eqs (26) and (27) gives:

$$\frac{\partial\psi_n}{\partial x} \simeq \frac{\psi_{ne} - \psi_{nw}}{2k} \tag{28}$$

ψ_{ne} and ψ_{nw} may be obtained from Taylor expansions about ψ'_e and ψ'_w:

$$\psi_{nw} \simeq \psi'_w + (h_w - S_1)\frac{\partial\psi'_w}{\partial r} + \frac{(h_w - S_1)^2}{2}\frac{\partial^2\psi'_w}{\partial r^2} \tag{29}$$

$$\psi_{ne} \simeq \psi'_e + (h_e + S_2)\frac{\partial\psi'_e}{\partial r} + \frac{(h_e + S_2)^2}{2}\frac{\partial\psi'_e}{\partial r^2} \tag{30}$$

Using the conventional finite-difference approximations for the derivatives, and noting that $\psi_{wall} = 1$, ie $\psi'_{ne} = \psi_n = \psi'_{nw} = 1$, gives:

$$\psi_{nw} \simeq \psi'_w + \frac{(h_w - S_1)(1 - \psi'_{sw})}{2h_w} + \frac{(h_w - S_1)^2(1 - 2\psi'_w + \psi'_{sw})}{2h_w{}^2} \tag{31}$$

$$\psi_{ne} \simeq \psi'_e + \frac{(h_e + S_2)(1 - \psi'_{se})}{2h_e} + \frac{(h_e + S_2)^2(1 - 2\psi'_e + \psi'_{se})}{2h_e{}^2} \tag{32}$$

The wall velocity gradient is obtained by applying the central difference approximation about obtained values of wall velocity. The grid values of the wall velocity gradient are used directly as a boundary condition in the following integral treatment of the wall boundary flow.

Calculations were carried out on a Prime 750 computer. Some of the program run characteristics are given in Table 1. The results presented in this paper were obtained using $\Delta x = 0.0025$ m, $N/K = 4$ and $Rp = 1.75$. This combination of run parameters represented an adequate compromise between run time and accuracy and provided sufficient wall points for the subsequent boundary layer analysis.

Boundary layer flow solution

The behaviour of the boundary layer from nozzle inlet to outlet is predicted using a modification of the method described by Au[3]. Au found that his experimental results on the change in mass flow rate of the axisymmetric boundary layer in a venturi meter could be correlated using a two-dimensional version of Head's entrainment model. The Reynolds number was in the range 1×10^5 to 5×10^5. Solutions to the boundary layer flow are obtained

Table 1 Computer program run characteristics

N	K	$\Delta X/L$	$(\Delta u/U)_{max}$	Number of iterations	approx. cpu time, min
12	12	0.016		69	2
20	20	0.010	+0.39%	69	8
32	32	0.00625	+0.12%	130	15
40	40	0.005	+0.06%	210	28

at the grid positions employed in the potential flow in terms of the shape factor, as described below.

In Fig 2 the flow element is bounded by the wall surface BC and an imagined inner surface AD of radius r_c. It is assumed that the flow is axisymmetric and the velocity at the edge of the boundary layer ($r=r_c$) is given by the potential flow solution at the wall.

From continuity, the mass flow across the annular surface AB is equal to the sum of the mass flows from the cylindrical surface AD and the annular surface CD. The mass flows have associated momentum fluxes and the change of momentum flux in the x-direction in the element equals the sum of all the applied forces on the element. These applied forces consist of pressure forces on the surfaces AB and CD, the x-direction pressure force due to the sloping wall and x-direction force due to wall friction.

The x-direction force-momentum balance may be written:

$$\frac{\mathrm{d}}{\mathrm{d}x}\int_{r_c}^{R} u^2 r\,\mathrm{d}r - U\frac{\mathrm{d}}{\mathrm{d}x}\int_{r_c}^{R} ur\,\mathrm{d}r + \frac{1}{2}\frac{\mathrm{d}P}{\mathrm{d}x}(R^2-r_c^2) + R\tau_w = 0 \tag{33}$$

For the potential flow outside the boundary layer

$$\frac{1}{\rho}\frac{\mathrm{d}p}{\mathrm{d}x} = -U\frac{\mathrm{d}U}{\mathrm{d}x} \tag{34}$$

Using Eq (34) together with the definitions of the axisymmetric boundary layer displacement, δ^*, and momentum thickness, θ:

$$\delta^*/R(1-\delta^*/2R) = \int_{r_c}^{R}(1-u/U)r/R\,\mathrm{d}r/R \tag{35}$$

$$\theta/R(1-\theta/2R) = \int_{r_c}^{R}(u/U)(1-u/U)r/R\,\mathrm{d}r/R \tag{36}$$

The equation of motion may be expressed in dimensionless form as:

$$\frac{\mathrm{d}\theta}{\mathrm{d}x} = \frac{R}{R-\theta}\left\{\left[\frac{\theta^2}{2RU}(H^2+2) - \frac{\theta}{U}(H+2)\right]\frac{\mathrm{d}U}{\mathrm{d}x} - \frac{\theta}{R}\frac{\mathrm{d}R}{\mathrm{d}x} + \frac{C_f}{2}\right\} \tag{37}$$

where the shape factor,

$$H = \delta^*/\theta \tag{38}$$

and

$$C_f = \tau_w/0.5\rho U^2 \tag{39}$$

Au[3] uses the Ludwig–Tillmann equation[9] for skin friction coefficient:

$$C_f = 0.246(10)^{-0.678H} Re_\theta^{-0.268} \tag{40}$$

White[10] reports that Eq (40) correlates available data to within $\pm 10\%$ but concludes that the following expression is to be preferred, with an accuracy of $\pm 3\%$:

$$C_f = 0.3\exp(-1.33H)(\ln Re_\theta)^{(-1.74-0.31H)} \tag{41}$$

Evaluation of the shape factor, H, requires an auxiliary entrainment equation which describes the interaction between the potential flow and the boundary layer flow for all states of the boundary layer (laminar or turbulent). Au[3] correlated boundary layer mass flow in terms of shape factor for venturi meters. This correlation may be used together with the boundary condition imposed by the potential flow solution to solve the equation of motion of the boundary layer. The method of solution involves seeking a value of H which will simultaneously satisfy the equation of motion and the entrainment equation.

$$\dot{m} = 2\pi\int_{r_c}^{R}\rho ur\,\mathrm{d}r \tag{42}$$

Using this definition, the mass flow rate in the boundary layer per unit circumferential length of nozzle wall is then:

$$\dot{M} = \rho UH'\theta[1-\theta(H'+2H)/2R] \tag{43}$$

where $H'=(\delta-\delta^*)/\theta$. The rate of entrainment is then given by:

$$\frac{\mathrm{d}\dot{M}}{\mathrm{d}x} = \frac{\mathrm{d}}{\mathrm{d}x}\left[\rho UH'\theta\left\{1-\frac{\theta(H'+2H)}{2R}\right\}\right] \tag{44}$$

letting

$$\eta = H'[1-\theta(H'+2H)/2R] \tag{45}$$

Introducing Au's correlation, Eq (43) may be written:

$$\frac{\mathrm{d}}{\mathrm{d}x}(U\theta\eta) = U\phi(\eta) \tag{46}$$

Differentiating, the entrainment equation becomes:

$$\theta\frac{\mathrm{d}\eta}{\mathrm{d}x} + \eta\frac{\mathrm{d}\theta}{\mathrm{d}x} + \frac{\theta\eta}{U}\frac{\mathrm{d}U}{\mathrm{d}x} - \phi = 0 \tag{47}$$

Au determined $\phi(\eta)$ empirically and related $\phi(\eta)$ to a single argument of shape factor, H, as follows:

$$\phi(H) = A_1H^3 + A_2H^2 + A_3H + A_4 \tag{48}$$

$$H = B_1\eta^3 + B_2\eta^2 + B_3\eta + B_4 \tag{49}$$

where $A_1 = 0.0090507$
$A_2 = -0.041917$
$A_3 = 0.0688713$
$A_4 = -0.0379579$
$B_1 = 8.23242\times10^{-5}$
$B_2 = 0.00636019$
$B_3 = -0.131286$
$B_4 = 2.04229$

A modified Adams–Moulton predictor-corrector technique was used to solve simultaneously the boundary layer flow equations and the entrainment equation. The boundary layer solution yields the skin friction coefficient distribution along the nozzle wall from which the laminar sublayer thickness may be determined. The sublayer thickness, S, is defined such that:

$$y^+ = 5 \tag{50}$$

ie

$$\frac{yv^*}{\nu} = 5 \qquad \text{where } v^* = \left\{\frac{\tau_w}{\rho}\right\}^{1/2} \tag{51}$$

Using the definition of skin friction coefficient,

$$S = \frac{5(2\nu)^{1/2}}{U(C_f)^{1/2}} \tag{52}$$

In fully relaminarized boundary layers the inner or viscous dominated region may be considerably thicker than for turbulent flow under equivalent conditions. It is likely, therefore, that sublayer thicknesses defined by Eq (52) represent a lower limit for some nozzle flows.

Problem specifications

The foregoing analysis is applicable to the design of any nozzle. The implementation of the method is exemplified below by reference to the procedure adopted in the design of nozzles for the mining of china clay.

Choice of geometry

Limitations imposed by the clay mining application lead to a general nozzle form consisting of a cubic arc matched to a final straight taper cone as shown in Fig 3. In order to determine the minimum acceptable nozzle length, ie that which minimizes exit boundary layer thickness and boundary layer separation near the inlet, a range of nozzle aspect ratios, $1 < L_t/D < 3.5$, was considered.

When choosing a nozzle geometry it is as well to bear in mind the findings of Ramjee and Hussain[5]. They studied the transformation of turbulence in nozzle flow and recommended certain desirable features which should be incorporated into nozzle geometry in order to avoid amplification of lateral turbulence levels. Generally a nozzle should create a gradual initial acceleration and should provide a high pressure gradient at the exit.

Given the values of D, d_o, β and L_t, L_f was chosen to avoid a point of inflection in the cubic arc portion of the nozzle contour. This constraint leads to a relatively simple nozzle shape and eliminates the possibility of separation and/or cavitation at the entrance to the final taper section. Selecting L_f too large or too small leads to a point of inflection in the cubic contour.

A nozzle diameter of 31.75 mm (1.25 inch) was selected for the study since it provided an acceptable contraction ratio, C_r, of 10.25, inch conjunction with a 101.6 mm (4 inch) diameter monitor barrel, and was a standard in the clay industry.

Flow inlet conditions

The range of flow conditions encountered in the clay industry was $3 \times 10^5 < Re_i < 5 \times 10^5$, $87 < Q_o < 175$, 527 kPa $< P_o <$ 2850 kPa. These conditions are sufficient to permit the potential flow solution to be obtained if some assumption about the shape of the inlet and outlet velocity profiles is made. For the present purposes uniform profiles were assumed. The potential flow solution must provide enough data along the wall for consumption by the boundary layer analysis. For this purpose, and for reasons of accuracy of the finite difference scheme, an axial step length of 0.0025 m, a grid parameter of $N/K = 4$ and a relaxation parameter of $R =$ 1.75 were found to be appropriate.

The inlet conditions for the boundary layer solution were estimated from the upstream flow conditions peculiar to clay monitors. The work of Ward-Smith[11] and Klein[12] is particularly useful in the estimation of the starting required values of shape factor and

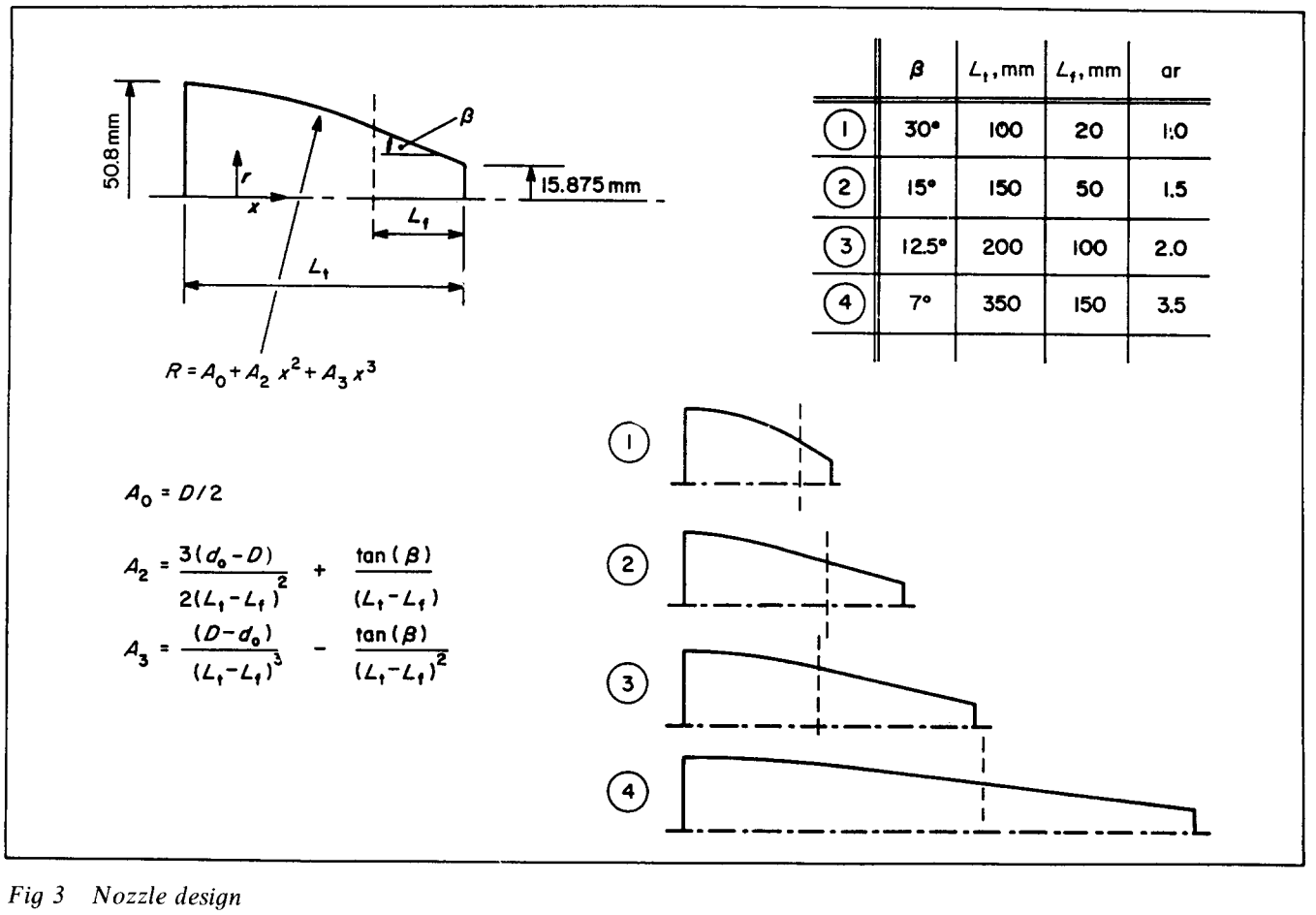

	β	L_t, mm	L_f, mm	ar
1	30°	100	20	1:0
2	15°	150	50	1.5
3	12.5°	200	100	2.0
4	7°	350	150	3.5

Fig 3 Nozzle design

entrainment function. Typical mid-range values used in the present study were $\theta = 0.002$ m, $\eta = 2$, $H = 1.8$.

Results

Major design faults can be avoided on the basis of the potential flow solution alone. In this context the pressure gradient parameter is of considerable utility:

$$K_p = \frac{v}{U^2}\frac{dU}{dx} \tag{53}$$

According to Schraub and Kline[4] the value of this parameter may be used to predict the onset of flow laminarization. According to Weber[13] it may also be used to predict the onset of flow separation using the following correlation:

$$K_p Re_\theta^{1.163} = -0.0319 \tag{54}$$

where $Re_\theta = \theta U/v$ is the local momentum thickness Reynolds number.

Fig 4 shows the distribution of the pressure gradient parameter calculated from the potential flow analysis for the four nozzles shown in Fig 3, for a particular inlet flow and pressure. The minima in the distributions near the inlet correspond to points of maximum unfavourable pressure gradient, and hence are points at which flow separation is most likely. The maxima in the distributions occurs in the region of maximum acceleration, and this is where laminarization of a turbulent layer is most likely. It is therefore to be expected that nozzle Design 1 would produce a jet with a boundary surface which would undergo some degree of reversion to turbulence. According to Hoyt and Taylor[6] this situation must be avoided if maximum jet coherence is to be achieved. The existence of an optimum flow rate for nozzles, demonstrated by Hatton and Osborne[8], may now be interpreted in terms of the increasing laminarization of the wall boundary layer and the subsequent transition to turbulence as the flow leaves the nozzle.

The finite values of the pressure gradient parameter at the nozzle exits are created by the convergent shape at the exit of all designs. This is a desirable feature since the possibility of cavitation caused by a decelerating flow is avoided.

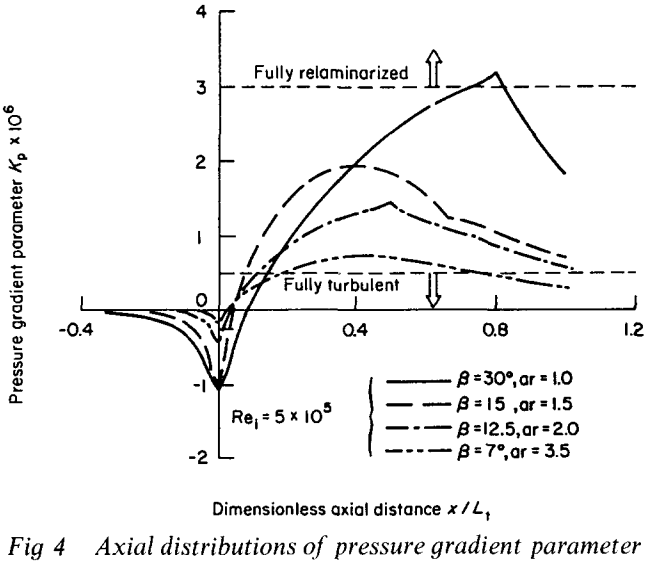

Fig 4 Axial distributions of pressure gradient parameter

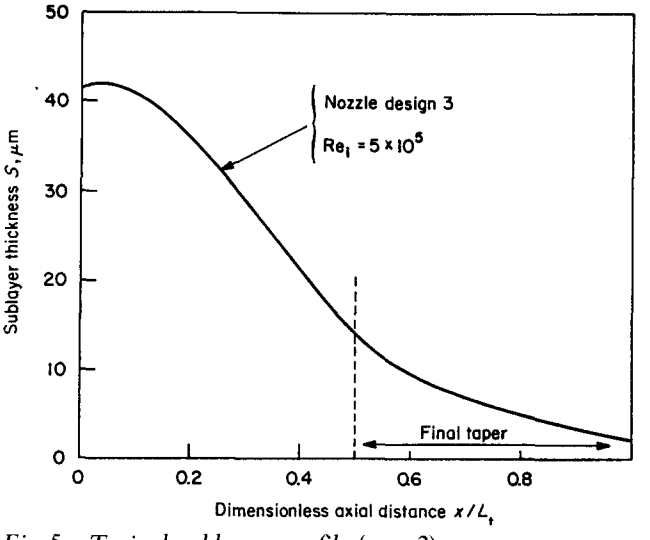

Fig 5 Typical sublayer profile (ar = 2)

On the basis of results similar to those shown in Fig 4 one may choose a nozzle geometry for more detailed examination. For example, Design 3 showed promise for the whole range of flow conditions expected in the mining application. Using the wall conditions predicted by the potential flow analysis, the boundary layer analysis was carried out for a range of values of the inlet boundary layer parameters. An example of the information available from such an analysis is shown in Fig 5, which is the variation in the sublayer thickness calculated from Eq (52). This prediction may be used as a guide to the surface finish requirements of the inner nozzle walls to ensure hydraulically smooth flow. The degree of surface finish needed will vary with the nozzle inlet conditions. For example, if the nozzle pressure is increased then the sublayer will become thinner. Surface protrusions which penetrate the sublayer near the nozzle exit may create local cavitation and so cause jet disruption.

Discharge coefficients

In the majority of experiments conducted to investigate water jets, the only available indication of nozzle flow phenomena is given by the coefficient of discharge C_d. Many attempts have been made in the past to predict discharge coefficients. In spite of more rigorous formulations of C_d in terms of exit boundary layer parameters for nozzles and venturi-meters by Benedict and Wyler[4] and Au[3] respectively, the approximation to the original equation of Rivas and Shapiro[15] used by Hall[16] is sufficiently accurate for a parallel exit section nozzle:

$$C_d = (1 - 4\delta^*/d_o) \tag{55}$$

Eq (55) cannot be used for nozzles of the kind considered in this paper, since the nozzle exit flow is non-parallel. Uniform parallel flow is only achieved downstream from the nozzle exit, at the vena-contracta. An effective method of estimating the discharge coefficient of tapered exit section nozzles is provided by the work of Gurevich[17]. For nozzles of the design considered in this paper the contraction coefficient C_c $(= d_{j_{min}}/d_o)$ may be estimated from Fig 6 and used in the following equation to estimate C_d.

$$C_d = C_c^2/[1 - (C_c d_o/D)^4]^{0.5} \tag{56}$$

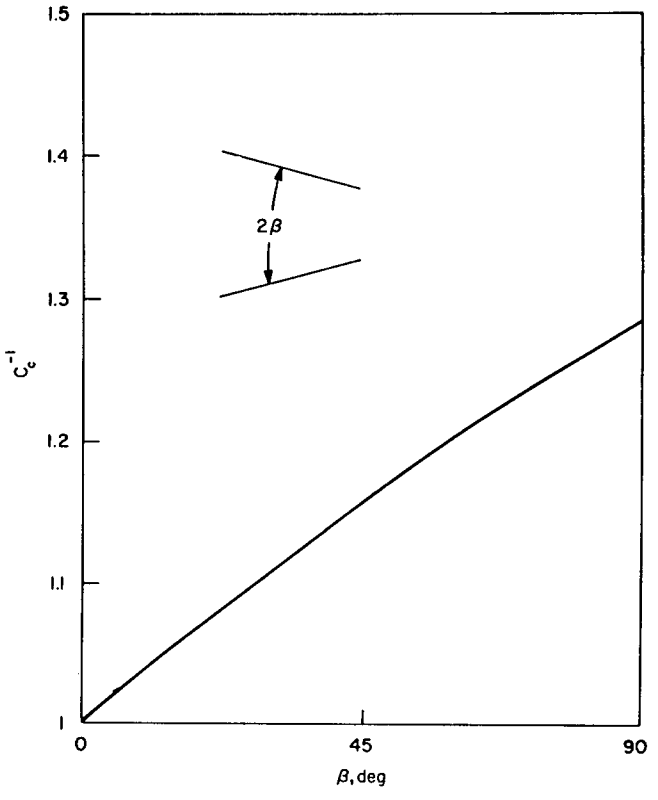

Fig 6 Contraction coefficient of a jet issuing from a tapered nozzle of half angle β

The discharge and contraction coefficients calculated in this way for the nozzles shown in Fig 3 are given in Table 2. This approach produces good agreement between measured and predicted nozzle flow rates.

Fig 7 shows the effect of nozzle aspect ratio on the exit displacement thickness of the wall boundary layer. The predictions for these nozzles are an order of magnitude lower than the exit displacement thicknesses of around 600 μm implied from the reported discharge coefficients of Murakami and Katayama[7]. This is attributable to the shape of the nozzle exit region.

Conclusions

The simple analysis described in this paper, together with empirical correlations for accelerated flows, may be used to examine the flow in arbitrarily shaped nozzles as a function of inlet flow conditions. The results of such analysis help to piece together fragmentary empiricisms on nozzle and jet flows.

When used in conjunction with the pressure gradient parameter, the potential flow analysis may be used to select those nozzle geometries which are most likely to produce the thinnest and best behaved boundary layers. Such nozzles are, in turn, most likely to produce jets with a long potential core.

The boundary layer analysis provides a guide to surface finish requirements so that hydraulically smooth flow throughout the nozzle may be ensured.

Acknowledgements

The authors gratefully acknowledge the financial assistance of the SERC and ECLP (plc), St. Austell, Cornwall.

Table 2 Discharge and contraction coefficients calculated for nozzles

β°	C_c	C_d
30	0.902	0.814
15	0.946	0.895
12.5	0.957	0.916
7	0.973	0.947

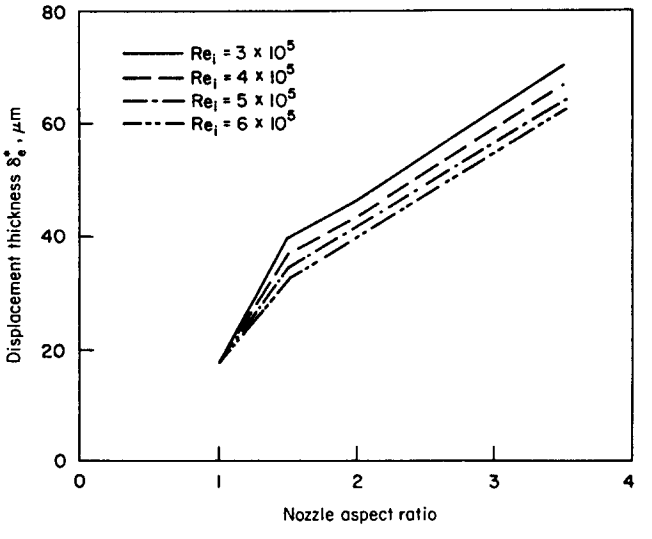

Fig 7 Effect of nozzle aspect ratio on exit displacement thicknesses

References

1. **Jackson M. K.** *Two-phase Characteristics of Turbulent Water Jets. PhD thesis, 1984, Exeter University, UK.*
2. **Lohn P. D. and Brent D. A.** *Improved Mineral Excavation Nozzle Design Study. TWR Systems and Energy Report No 27752-6003-TU-00, 1976 (for the U.S. Bureau of Mines)*
3. **Au S. R.** *Boundary Layer Development in Venturimeters. PhD thesis, 1972, University of Wales, UK*
4. **Schraub F. A. and Kline S. J.** *A Study of the Structure of the Turbulent Boundary Layer with and without Longitudinal Pressure Gradients. Report MD-12, 1965, Thermosciences Division, Stanford University, USA*
5. **Ramjee V. and Hussain A. K. M. F.** Influence of the axisymmetric contraction ratio on free stream turbulence. *Trans. ASME, J. Fluids Engng, 1976,* **98**, *506–515*
6. **Hoyt J. W. and Taylor J. J.** Waves on water jets. *J. Fluid Mech., 1977,* **83**, *part 1, 119–127*
7. **Murakami M. and Katayama K.** Discharge coefficients of fire nozzles. *Trans. ASME, J. Basic Engng, 1966,* **88**, *706–716*
8. **Hatton A. P. and Osborne M. J.** The trajectories of large fire fighting jets. *Int. J. Heat and Fluid Flow, 1979,* **1**(*1*), *37–41*
9. **Ludwieg H. and Tillmann W.** *Investigations of the Wall Shearing Stress in Turbulent Boundary Layers. NACA TM 1285, 1949*
10. **White F. M.** *Viscous Fluid Flow. McGraw-Hill, 1974*
11. **Ward-Smith A. J.** *Internal Fluid Flow. Clarendon Press, Oxford, 1980*
12. **Klein A.** Review: turbulent developing pipe flow. *Trans. ASME, J. Fluids Engng, 1981,* **103**, *243–249*
13. **Weber H. E.** Boundary layer calculation for analysis and design. *Trans. ASME, J. Fluids Engng, 1978,* **100**, *232–236*
14. **Benedict R. P. and Wyler J. S.** Analytical and experimental studies of ASME flow nozzles. *Trans. ASME, J. Fluids Engng, 1978,* **100**, *265–275*
15. **Rivas M. A. and Shapiro A. H.** On the theory of discharge coefficients for round entrance flow meters and venturis. *Trans. ASME, J. Basic Engng, 1956,* **78**, *489*
16. **Hall G. W.** Application of boundary layer theory to explain some nozzle and venturimeter flow peculiarities. *Proc. Instn. Mech. Engrs., 1959,* **173**(*36*), *837–870*
17. **Gurevich M. I.** *Theory of Jets in Ideal Fluids. Academic Press, 1965*